

Learning rewards for robotic ultrasound scanning using probabilistic temporal ranking

Michael Burke, Katie Lu, Daniel Angelov, Artras Straiys, Craig Innes, Kartic Subr, Subramanian Ramamoorthy
Institute of Perception, Action and Behaviour

University of Edinburgh, Edinburgh, UK

Email: {michael.burke, k.r.lu, d.angelov, a.straiys, craig.innes, k.subr, s.ramamoorthy}@ed.ac.uk

Abstract—This paper addresses a common class of problems where a robot learns to perform a discovery task based on example solutions, or *human demonstrations*. As an example, this work considers the problem of ultrasound scanning, where a demonstration involves an expert adaptively searching for a satisfactory view of internal organs, vessels or tissue and potential anomalies while maintaining optimal contact between the probe and surface tissue. Such problems are often solved by inferring notional *rewards* that, when optimised for, result in a plan that mimics demonstrations. A pivotal assumption, that plans with higher reward should be exponentially more likely, leads to the de facto approach for reward inference in robotics. While this approach of maximum entropy inverse reinforcement learning leads to a general and elegant formulation, it struggles to cope with frequently encountered sub-optimal demonstrations. In this paper, we propose an alternative approach to cope with the class of problems where sub-optimal demonstrations occur frequently. We hypothesise that, in tasks which require discovery, successive states of any demonstration are progressively more likely to be associated with a higher reward. We formalise this *temporal ranking* approach and show that it improves upon maximum-entropy approaches to perform reward inference for autonomous ultrasound scanning, a novel application of learning from demonstration in medical imaging.

I. INTRODUCTION

The ability to teach robotic agents using expert demonstration of tasks promises exciting developments across several sectors of industry. Indirect imitation learning approaches formulate this as a search problem within a solution space of plans, where some notional (unknown) *reward function* induces the demonstrated behaviour. A key learning problem is then to estimate this reward function. This *reward inference* approach is commonly known as inverse reinforcement learning (IRL) [34].

The IRL approach to apprenticeship learning [1] aims to match the frequency (counts) of features encountered in the learners behaviour with those observed in demonstrations. This technique provides necessary and sufficient conditions when the reward function is linear in the features encoding execution states, but results in ambiguities in associating optimal policies with reward functions or feature counts. An elegant reformulation of this using the principle of maximum entropy resolves ambiguities and results in a single optimal stochastic policy. Methods for maximum-entropy IRL [42, 40, 23] identify reward functions using maximum likelihood estimation, typically under the assumption that the probability of seeing a given trajectory is proportional to the exponential of the

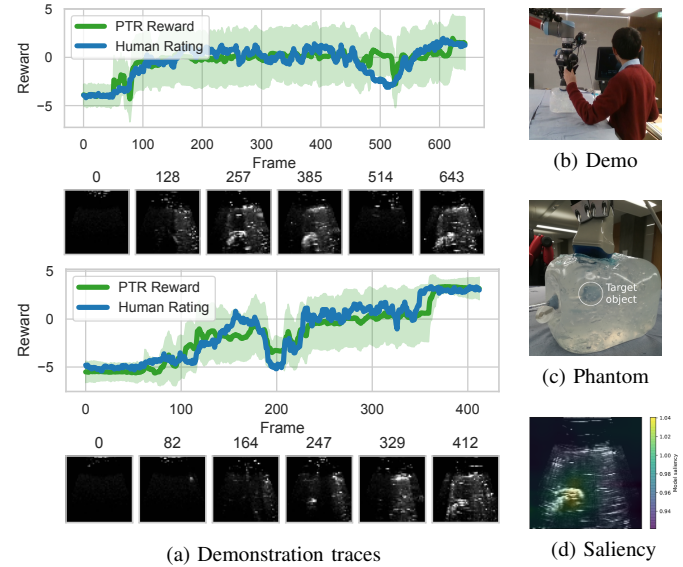


Fig. 1. This work introduces a temporal ranking strategy to learn reward functions (a) from human demonstrations (b) for autonomous ultrasound scanning. Probabilistic temporal ranking can learn to identify non-monotonically increasing rewards from demonstration image sequences containing exploratory actions, and successfully associates ultrasound features corresponding to a target object (c) with rewards (d).

total reward along a given path. Unfortunately, these methods are fundamentally frequentist and thus struggle to cope with *repetitive sub-optimal demonstrations*, as they assume that frequent appearance implies relevance. i.e. If a feature is seen repeatedly across demonstration trajectories, it is deemed valuable, as are policies that result in observations of these features. This makes these approaches unsuitable for a broad class of tasks that require *exploratory actions* or environment identification during demonstration. e.g. an expert using an ultrasound scan to locate a tumour (Fig. 1).

Obtaining useful ultrasound images requires contact with a deformable body (see Fig. 2) at an appropriate position and contact force, with image quality affected by the amount of ultrasound gel between the body and the probe, and air pockets that obscure object detection. This means that human demonstrations are frequently and inherently sub-optimal, requiring that a demonstrator actively search for target objects, while attempting to locate a good viewpoint position and appropriate contact force. This class of demonstration violates many of the assumptions behind maximum entropy IRL.

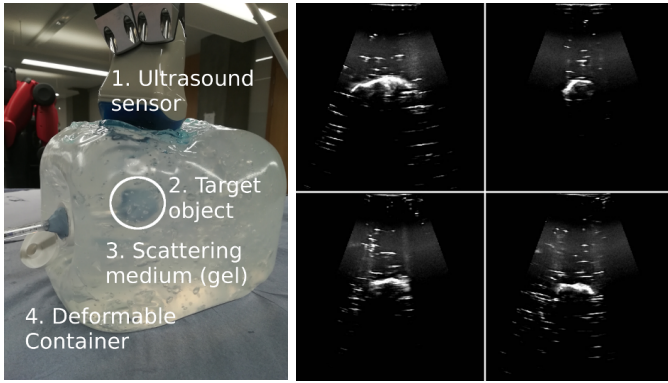


Fig. 2. This work considers the task of learning to search for and capture an image of a target object (2.) suspended in a scattering material (3.) housed within a deformable container (4.). Our goal is to learn a reward signal from demonstrations that allows us to move an ultrasound sensor (1.) to positions that produce clear images of the target object. High quality ultrasound images (right) captured by a human demonstrator show high intensity contour outlines, centre the target object of interest, and generally provide some indication of target object size.

This work introduces a temporal ranking model of reward that addresses these limitations. Instead of assigning reward based on the maximum entropy model, we attribute reward using a ranking model. Here, we assume that, in general, an expert acts to improve their current state. This means that it is likely that a state at a later stage in a demonstrated trajectory is more important than one seen at an earlier stage. We make use of this fact to generate feature pairs and train a probabilistic pairwise ranking model from image pixels.

Importantly, the proposed pairwise ranking scheme is able to handle cases where this temporal improvement is unsteady and non-monotonic, with intermediate performance dips.

Experimental results show that this pairwise feature ranking successfully recovers reward maps from demonstrations in tasks requiring significant levels of exploration alongside exploitation (where maximum entropy IRL fails), and obtains similar performance to maximum entropy inverse IRL when optimal demonstrations are available.

We illustrate the value of our approach in a challenging ultrasound scanning application, where demonstrations inherently contain a searching process, and show that we can train a model to find a tumour-like mass in an imaging phantom¹. Ultrasound imaging is a safe and low cost sensing modality of significant promise for surgical robotics, and is already frequently used for autonomous needle steering and tracking [25, 12]. Autonomous visual servoing systems have been proposed in support of teleoperated ultrasound diagnosis [2, 24], but these techniques rely on hand designed anatomical target detectors. The scanner introduced in this work is fully autonomous, and relies entirely on a reward signal learned from demonstration, in what we believe is a first for medical imaging. Importantly, the proposed pairwise ranking model provides more signal for learning, as a greater number of comparisons can be generated from each demonstration trajectory.

¹An imaging phantom is an object that mimics the physical responses of biological tissue, and is commonly used in medical imaging to evaluate and analyse imaging devices.

This means that we can train a more effective prediction model from pixels than with maximum entropy IRL, which in turn opens up a number of avenues towards self-supervised learning for medical imaging and diagnosis.

In summary, the primary contributions of this paper are

- a trajectory state ranking reward model that allows for reward inference from sub-optimal, high dimensional exploratory demonstrations, and
- a method for autonomous ultrasound scanning using image sequence demonstrations.

II. RELATED WORK

As mentioned previously, apprenticeship learning [1] is an alternative to direct methods of imitation learning [4] or behaviour cloning, and is currently dominated by approaches making use of maximum entropy assumptions.

A. Maximum entropy inverse reinforcement learning

Maximum entropy or maximum likelihood inverse reinforcement learning models the probability of a user preference for a given trajectory ζ as proportional to the exponential of the total reward along the path [42],

$$p(\zeta|r) \propto \exp\left(\sum_{s,a \in \zeta} r_{s,a}\right). \quad (1)$$

Here, s denotes a state, a an action, and $r_{s,a}$ the reward obtained for taking an action in a given state. It is clear that this reward model can be maximised by any number of reward functions. Levine et al. [23] use a Gaussian process prior to constrain the reward, while Wulfmeier et al. [40] back-propagate directly through the reward function using a deep neural network prior. Maximum entropy inverse reinforcement learning approaches are typically framed as iterative policy search, where policies are identified to maximise the reward model. This allows for the incorporation of additional policy constraints and inductive biases towards desirable behaviours, as in relative entropy search [6], which uses a relative entropy term to keep policies near a baseline, while maximising reward feature counts. Maximum entropy policies can also be obtained directly, bypassing reward inference stages, using adversarial imitation learning [20, 16, 17, 18], although reward prediction is itself useful for medical imaging applications and safety concerns limit online policy search here. In contrast, this paper focuses primarily on developing an improved reward model that serves as a replacement for the maximum entropy assumption. In light of this, we focus on reward inference directly, and leave policy search extensions using the proposed approach to future work.

Although maximum entropy IRL is ubiquitous, alternative reward models have been proposed. For example, Angelov et al. [3] train a neural reward model using demonstration sequences, to schedule high level policies in long horizon tasks. Here, they capture overhead scene images, and train a network to predict a number between 0 and 1, assigned in increasing order to each image in a demonstration sequence. This ranking approach is similar to the pairwise ranking method we propose, but, as will be shown in later results, is limited by its

rigid assumption of linearly increasing reward. Majumdar et al. [28] propose flexible reward models that explicitly account for human risk sensitivity. Time contrasted networks [36] learn disentangled latent representations of video using time as a supervisory signal. Here, time synchronised images taken from multiple viewpoints are used to learn a latent embedding space where similar images (captured from different viewpoints) are close to one another. This embedding space can then be used to find policies from demonstrations. Time contrasted networks use a triplet ranking loss, and are trained using positive and negative samples (based on frame timing margins).

B. Preference-based inverse reinforcement learning

Preference-based ranking of this form is widely used in inverse reinforcement learning to rate demonstrations [39], and preference elicitation [7] is a well established area of research. For example, Brochu et al. [8] use Bayesian optimisation with a pairwise ranking model to allow users to procedurally generate realistic animations. Lopes et al. [27] actively query demonstrators to learn reward functions. Sugiyama et al. [37] use preference-based inverse reinforcement learning for dialog control. Here, dialog samples are annotated with ratings, which are used to train a preference-based reward model. These preference elicitation approaches are effective, but place a substantial labelling burden on users. In this work, we consider the non-interactive learning case where we are required to learn directly from unlabelled observation traces.

Brown et al. [9] make use of a preference ranking approach to improve robot policies through artificial trajectory ranking using increasing levels of injected noise. Unlike Brown et al. [9], which uses preference ranking over trajectories, our work uses preference ranking within trajectories, under the assumption that a demonstrator generally acts to improve or maintain their current state. We use a Bayesian image ranking model [10] that accounts for potential uncertainty in this assumption, and is less restrictive than the linear increasing model of Angelov et al. [3]. Bayesian ranking models [14] are common in other fields – for example, TrueSkillTM [19] is widely used for player performance modelling in online gaming settings, but has also been applied to train image-based style classifiers in fashion applications [21] and to predict the perceived safety of street scenes using binary answers to the question “Which place looks safer?” [32].

C. Active viewpoint selection

Given an appropriate reward model, autonomous ultrasound scanning requires a policy that balances both exploration and exploitation for active viewpoint selection or informative path planning. Research on active viewpoint selection is concerned with agents that choose viewpoints which optimise the quality of the visual information they sense. Similarly, informative path planning involves an agent choosing actions that lead to observations which most decrease uncertainty in a model. Gaussian processes (GP) are frequently used for informative path planning because of their inclusion of uncertainty, data-efficiency, and flexibility as non-parametric models.

Binney and Sukhatme [5] use GPs with a branch and bound algorithm, while Cho et al. [13] perform informative path planning using GP regression and a mutual information action selection criterion. More general applications of GPs to control include PILCO [15], where models are optimised to learn policies for reinforcement learning control tasks, and the work of Ling et al. [26], which introduces a GP planning framework that uses GP predictions in H-stage Bellman equations.

These Bayesian optimisation schemes are well-established methods for optimisation of an unknown function, and have been applied to many problems in robotics including policy search [30], object grasping [41], and bipedal locomotion [11].

By generating policies dependent on predictions for both reward value and model uncertainty, Bayesian optimisation provides a mechanism for making control decisions that can both progress towards some task objective and acquire information to reduce uncertainty. GPs and Bayesian optimisation are often used together, with a GP acting as the surrogate model for a Bayesian optimisation planner, as in the mobile robot path planning approaches of [31] and [29]. Our work takes a similar approach, using GP-based Bayesian optimisation for path planning in conjunction with the proposed observation ranking reward model.

III. PROBABILISTIC TEMPORAL RANKING

This paper incorporates additional assumptions around the structure of demonstration sequences, to allow for improved reward inference. We introduce a reward model that learns from pairwise comparisons sampled from demonstration trajectories. Here we assume that an observation or state seen later in a demonstration trajectory should typically generate greater reward than one seen at an earlier stage. Below, we first describe a fully probabilistic ranking model that allows for uncertainty quantification and inference from few demonstrations, before introducing a maximum likelihood approximation that can be efficiently trained in a fully end-to-end fashion, and is more suited to larger training sets.

A. Fully probabilistic model

We build on the pairwise image ranking model of Burke et al. [10], replacing pre-trained object recognition image features with a latent state, $\mathbf{x}_t \in \mathbf{R}^d$, learned using a convolutional variational autoencoder (CVAE),

$$\mathbf{x}_t \sim \mathcal{N}(\mu(\mathbf{Z}_t), \sigma(\mathbf{Z}_t)), \quad (2)$$

that predicts mean, $\mu(\mathbf{Z}_t) \in \mathbf{R}^d$, and diagonal covariance, $\sigma(\mathbf{Z}_t) \in \mathbf{R}^{d \times d}$, for input observation $\mathbf{Z}_t \in \mathbf{R}^{w \times h}$ captured at time t (assuming image inputs of dimension $w \times h$).

Rewards $r_t \in \mathbf{R}^1$ are modelled using a Gaussian process prior,

$$\begin{bmatrix} r' \\ r_t \end{bmatrix} \sim \mathcal{N} \left(\mathbf{0}, \begin{bmatrix} K(\mathbf{X}', \mathbf{X}') + \Sigma_n & K(\mathbf{X}', \mathbf{x}_t) \\ K(\mathbf{x}_t, \mathbf{X}') & K(\mathbf{x}_t, \mathbf{x}_t) \end{bmatrix} \right). \quad (3)$$

Here, we use \mathbf{X}' and r' to denote states and reward pairs corresponding to training observations. $\mathbf{X}' \in \mathbf{R}^{N \times d}$ is a matrix formed by vertically stacking N latent training states,

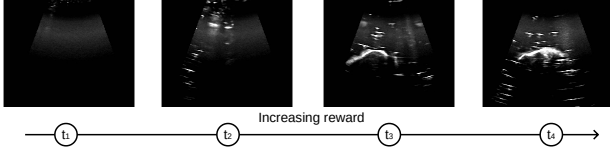


Fig. 3. Time is used as a supervisory signal, by sampling image pairs at times t_i, t_j , and setting $g = 1$ if $t_i > t_j$, $g = 0$ otherwise.

and $K(\mathbf{X}', \mathbf{X}')$ a covariance matrix formed by evaluating a Matern32 kernel function

$$k(\mathbf{x}_t, \mathbf{y}_t) = \text{Matern32}(\mathbf{x}_t, \mathbf{y}_t, l), \quad \mathbf{x}_t, \mathbf{y}_t \in \mathbb{R}^d \quad (4)$$

for all possible combinations of latent state pairs $\mathbf{x}_t, \mathbf{y}_t$, sampled from the rows of \mathbf{X}' . $l \in \mathbb{R}^1$ is a length scale parameter with a Gamma distributed prior, $l \sim \Gamma(\alpha = 2.0, \beta = 0.5)$, and $\Sigma_n \in \mathbb{R}^{N \times N}$ is a diagonal heteroscedastic noise covariance matrix, with diagonal elements drawn from a Half Cauchy prior, $\Sigma_n \sim \text{HalfCauchy}(\beta = 1.0)$. At prediction time, reward predictions r_t for image observations \mathbf{Z}_t can be made by encoding the image to produce latent state \mathbf{x}_t , and conditioning the Gaussian in Equation (3) [38].

Using this model, the generative process for a pairwise comparison outcome, $g \in \{0, 1\}$, between two input observation rewards r_{t_1} and r_{t_2} at time steps t_1 and t_2 , is modelled using a Bernoulli trial over the sigmoid of the difference between the rewards,

$$g \sim \text{Ber}(\text{Sig}(r_{t_2} - r_{t_1})). \quad (5)$$

This Bernoulli trial introduces slack in the model, allowing for tied or even decreasing rewards to be present in the demonstration sequence.

B. Reward inference using temporal observation ranking

The generative model above is fit to demonstration sequences using automatic differentiation variational inference (ADVI) [22] by sampling N observation pairs $\mathbf{Z}_{t_1}, \mathbf{Z}_{t_2}$ from each demonstration sequence, which produce a comparison outcome $g = 1$ if $t_2 > t_1$, and $g = 0$ if $t_1 > t_2$.

Intuitively, this comparison test, which uses time as a supervisory signal (Fig. 3), operates as follows. Assume that an image captured at time step t_2 has greater reward than an image captured at t_1 . This means that the sigmoid of the difference between the rewards is likely to be greater than 0.5, which leads to a higher probability of returning a comparison outcome $g = 1$. Importantly, this Bernoulli trial allows some slack in the model – when the difference between the rewards is closer to 0.5, there is a greater chance that a comparison outcome of $g = 1$ is generated by accident. This means that the proposed ranking model can deal with demonstration trajectories where the reward is non-monotonic. Additional slack in the model is obtained through the heteroscedastic noise model, Σ_n , which also allows for uncertainty in inferred rewards to be modelled.

Inference under this model amounts to using the sampled comparison outcomes from a demonstration trajectory to find rewards that generate similar comparison outcomes, subject to the Gaussian process constraint that images with similar

TABLE I
AVERAGED TOTAL RETURNS USING VI POLICY TRAINED USING INFERRED REWARD FROM OPTIMAL DEMONSTRATIONS.

	Reward
GP-PTR-IRL	9.51 ± 4.92
GP-ME-IRL [23]	9.58 ± 4.90
GP-LTR-IRL [3]	7.39 ± 5.72

appearance should exhibit similar rewards. After inference, we make reward predictions by encoding an input image, and evaluating the conditional Gaussian process at this latent state.

We briefly illustrate the value of this probabilistic temporal ranking approach in exploratory tasks using two simple grid world experiments.

C. Grid world – optimal demonstrations

The first experiment considers a simple grid world, where a Gaussian point attractor is positioned at some unknown location. Our goal is to learn a reward model that allows an agent (capable of moving up, down, left and right) to move towards the target location. For these experiments, our state is the agent’s 2D grid location.

We generate 5 demonstrations (grid positions) from random starting points, across 100 randomised environment configurations with different goal points. We then evaluate performance over 100 trials in each configuration, using a policy obtained through tabular value iteration using the reward model inferred from the 5 demonstrations. This policy is optimal, as the target location is known, so for all demonstrations the agent moves directly towards the goal, as illustrated for the sample environment configuration depicted in Fig. 4.

Table I shows the averaged total returns obtained for trials in environments when rewards are inferred from optimal demonstrations using the probabilistic temporal ranking² (GP-PTR-IRL), a Gaussian process maximum entropy approach [23] (GP-ME-IRL) and an increasing linear model assumption [3] (GP-LTR-IRL). Value iteration is used to find a policy using the mean inferred rewards.

In the optimal demonstration case, policies obtained using both the maximum entropy and probabilistic temporal ranking approach perform equally well, although the pairwise ranking model assigns more neutral rewards to unseen states (Fig. 4). Importantly, as the proposed model is probabilistic, the uncertainty in predicted reward can be used to restrict a policy to regions of greater certainty by performing value iteration using an appropriate acquisition function instead of the mean reward. This implicitly allows for risk-based policies – by weighting uncertainty higher, we could negate the neutrality of the ranking model (risk-averse). Alternatively, we could tune the weighting to actively seek out uncertain regions with perceived high reward (risk-seeking).

D. Grid world – sub-optimal demonstrations

Our second experiment uses demonstrations that are provided by an agent that first needs to explore the environment, before exploiting it. Here, we use a Gaussian process

²We use PyMC3 [35] (GP-PTR-IRL) to build probabilistic reward models and ADVI [22] for model fitting.

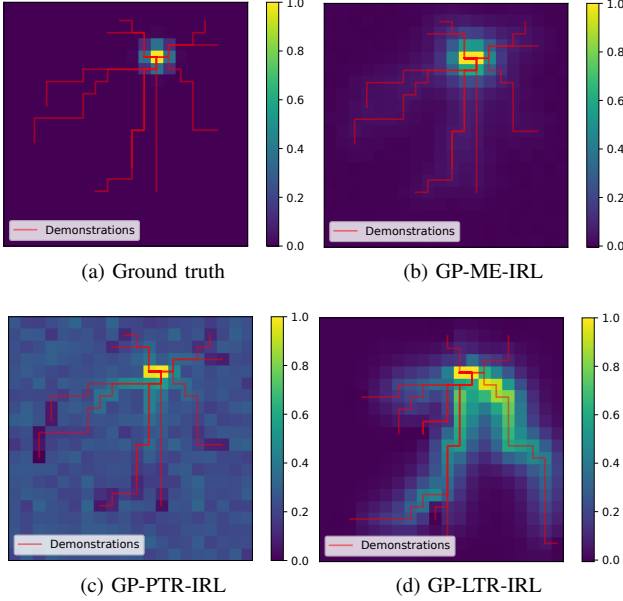


Fig. 4. Reward inference from **optimal** demonstrations. Demonstration trajectories are marked in red, and the colour map indicates the reward for each grid position. PTR and ME models have similar relative reward values, and policies trained using these rewards perform near identically. A linearly increasing reward model (LTR) attributes reward more evenly across a demonstration, resulting in sub-optimal policy performance here.

TABLE II
AVERAGED TOTAL RETURNS USING VI POLICY TRAINED USING INFERRED REWARD FROM SUB-OPTIMAL DEMONSTRATIONS.

	Reward
GP-PTR-IRL	7.42 ± 4.82
GP-ME-IRL [23]	3.31 ± 4.24
GP-LTR-IRL [3]	2.77 ± 4.30

model predictive control policy (see Section IV-A) to generate demonstrations, and repeat the experiments above. As shown in Fig. 5, this policy may need to cover a substantial portion of the environment before locating the target.

Table II shows the averaged total returns obtained for trials in environments when rewards are inferred from sub-optimal demonstrations using probabilistic temporal ranking, the Gaussian process maximum entropy approach and the linearly increasing reward assumption. Here, value iteration is used to find the optimal policy using the inferred rewards.

In this sub-optimal exploratory demonstration case, policies obtained using the maximum entropy approach regularly fail, while the probabilistic temporal ranking continues to perform relatively well. Fig. 5 shows a sample environment used for testing. The sub-optimal behaviour of the exploring model predictive control policies used for demonstration can result in frequent visits to undesirable states, which leads to incorrect reward attribution under a maximum entropy model. Probabilistic temporal ranking avoids this by using the looser assumption that states generally improve over time.

E. Maximum likelihood neural approximation

Given that learning from demonstration typically aims to require only a few trials, numerical inference under the fully

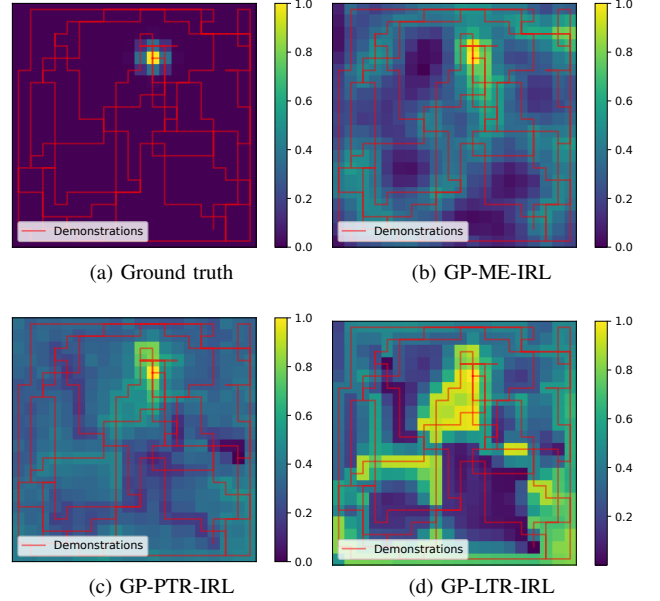


Fig. 5. Reward inference from **sub-optimal** demonstrations. Demonstration trajectories are marked in red, and the colour map indicates the reward for each grid position. Both the linearly increasing and maximum entropy reward models induce local maxima that result in sub-optimal policies.

Bayesian generative model described above is tractable, particularly if a sparse Gaussian process prior is used. However, in the case where a greater number of demonstrations or comparisons is available, we can perform maximum likelihood inference under the fully probabilistic model above in an end-to-end fashion, using the architecture in Fig. 6. Here, we can replace the Gaussian process with a single layer fully connected network (FCN), $r_\psi(\mathbf{x})$, with parameters ψ , since single layer FCN's are known to approximate Gaussian processes [33], and minimise a binary cross entropy loss over the expected comparison outcome alongside a variational autoencoder (VAE) objective,

$$\begin{aligned} \mathcal{LL} = & -\mathbb{E}_{\mathbf{x}_{t_1} \sim q_\theta} [\log p_\phi(\mathbf{Z}_{t_1} | \mathbf{x})] + \mathbb{KL}(q_\theta(\mathbf{x} | \mathbf{Z}_{t_1}) || p(\mathbf{x})) \\ & - \mathbb{E}_{\mathbf{x}_{t_2} \sim q_\theta} [\log p_\phi(\mathbf{Z}_{t_2} | \mathbf{x})] + \mathbb{KL}(q_\theta(\mathbf{x} | \mathbf{Z}_{t_2}) || p(\mathbf{x})) \\ & - \frac{1}{N} \sum_{i=1}^N g_i \log(h(g_i)) + (1 - g_i) \log(1 - h(g_i)) \quad (6) \end{aligned}$$

using stochastic gradient descent. Here, \mathcal{LL} denotes the overall loss, $p(\mathbf{x})$ is a standard normal prior over the latent space, $q_\theta(\mathbf{x} | \mathbf{Z}_{t_i})$ denotes the variational encoder, with parameters θ , $p_\phi(\mathbf{Z}_{t_i} | \mathbf{x})$ represents the variational decoder, with parameters ϕ , and $h(g)$ is the comparison output logit (sigmoid). g_i is a comparison outcome label, and \mathbf{Z}_{t_i} denotes a training sample image, with \mathbf{x}_t a sample from the latent space. Weight sharing is used for both the convolutional VAEs and FCNs.

Once trained, the reward model is provided by encoding the input observation, and then predicting the reward using the FCN. This allows for rapid end-to-end training using larger datasets and gives us the ability to backpropagate the comparison supervisory signal through the autoencoder, potentially allowing for improved feature extraction in support of reward modelling. However, this comes at the expense of

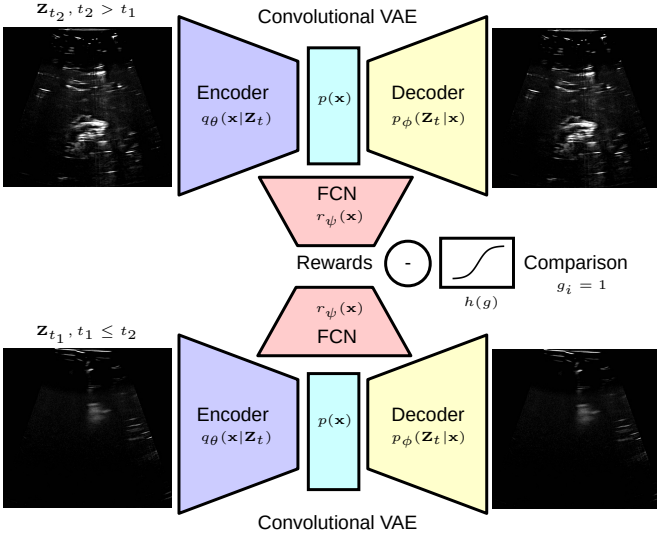


Fig. 6. Neural (maximum likelihood) model. Sampled images are auto-encoded, and a reward network predicts corresponding rewards, the sigmoid of the difference between these reward produces a comparison outcome probability. Weight sharing is indicated by colour. The network is trained jointly using a joint variational autoencoder and binary cross entropy loss.

uncertainty quantification, which is potentially useful for the design of risk-averse policies that need to avoid regions of uncertainty. We investigate these tradeoffs in the context of autonomous ultrasound scanning.

IV. AUTONOMOUS ULTRASOUND SCANNING

For our primary experiment, we demonstrate the use of probabilistic temporal ranking in a challenging ultrasound scanning application. Here, we capture 10 kinesthetic demonstrations of a search for a target object using a compliant manipulator, and use only ultrasound image sequences (2D trapezoidal cross-sectional scans) to learn a reward model. Our goal is to use this reward model within a control policy that automatically searches for and captures the best image of a tumour-like mass³ suspended within a deformable imaging phantom constructed using a soft plastic casing filled with ultrasound gel.

This task is difficult because it involves a highly uncertain and dynamic domain. Obtaining stable ultrasound images requires contact with a deformable imaging phantom at an appropriate position and contact force, with image quality affected by the thickness of the ultrasound gel between the phantom and the probe, while air pockets within the phantom object can obscure object detection. Moreover, since the phantom deforms, air pockets and gel can move in response to manipulator contact. This means that kinesthetic demonstrations are inherently sub-optimal, as they require that a demonstrator actively search for target objects, while attempting to locate a good viewpoint position and appropriate contact force. As in real-world medical imaging scenarios, the demonstrator is unable to see through the phantom object from above, so demonstrations are based entirely on visual feedback from an ultrasound monitor.

³A roughly 30 mm x 20 mm blob of Blu tack original in a container of dimensions 200 mm x 150 mm x 150 mm.

A. Gaussian process model predictive control

Although the proposed reward model can be used with any policy, we demonstrate its use by means of a Bayesian optimisation policy, selecting action $\hat{\mathbf{a}}_t$ that drives an agent to a desired state $\hat{\mathbf{s}}_t$, drawn from a set of possible states using an upper confidence bound objective function that seeks to trade off expected reward returns against information gain or uncertainty reduction.

Here, we learn a mapping between reward and end-effector positions using a surrogate Gaussian process model with a radial basis function kernel,

$$r_t \approx \mathcal{GP}(\mathbf{0}, \text{RBF}(\mathbf{s}_t)). \quad (7)$$

The Gaussian process is trained on pairs consisting of each visited state (in our experiments these are 3D Cartesian end-effector positions) and the corresponding reward predicted using the image-based reward model. Actions are then chosen to move to a desired state selected using the objective function,

$$\hat{\mathbf{s}}_t = \operatorname{argmax}_{\mathbf{s}_t} \mu(\mathbf{s}_t) - \beta\sigma(\mathbf{s}_t). \quad (8)$$

Here $\mu(\mathbf{s}_t)$, $\sigma(\mathbf{s}_t)$ are the mean and standard deviation of the Gaussian process, and β is a hyperparameter controlling the exploration exploitation trade-off of the policy. This objective function is chosen in order to balance the competing objectives of visiting states that are known to maximise reward with gaining information about values of states for which the model is more uncertain. In our ultrasound imaging application, actions are linear motions to a desired Cartesian state.

It should be noted that any policy can be used to optimise rewards inferred using probabilistic temporal ranking. We selected a Bayesian optimisations strategy for online experiments due to its prevalence in active viewpoint selection literature, and because of its ability to deal with uncertainty in state rewards arising from the dynamic structure of the deformable imaging phantom.

B. Reward inference evaluation

Fig. 1 shows predicted reward sequences for sample expert demonstration traces held out from model training. It is clear that the ranking reward model captures the general improvements in image quality that occur as the demonstrator searches for a good scanning view, and that some searching is required before a good viewpoint is found. Importantly, the slack in the pairwise ranking model, combined with the model assumption that similar images result in similar rewards, allows for these peaks and dips in reward to be modelled, as probabilistic temporal ranking does not assume monotonically increasing rewards.

We qualitatively assessed the image regions and features identified using the reward model using saliency maps (Fig. 1d), which indicated that the proposed approach has learned to associate the target object with reward.

In order to quantitatively evaluate the performance of probabilistic temporal ranking for autonomous ultrasound imaging, approximately 5000 ultrasound images from a set of 10 demonstration sequences were ordered in terms of human

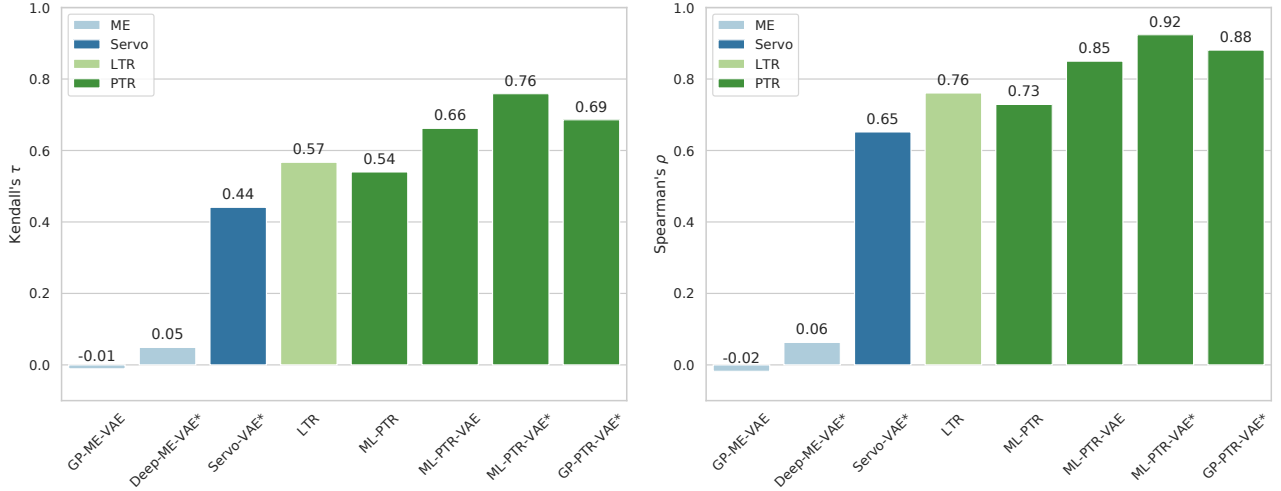


Fig. 7. Reward model association with human image ratings shows that temporal ranking (green) reward inference models strongly agree with human preferences. A Spearman rank correlation of $\rho = 1$ indicates an identical rank or ordering, while $\rho = -1$ indicates a completely opposing order. Similarly, Kendall's $\tau = 1$ indicates that the relative rank assigned to images is identical to that assigned by the human annotator, while $\tau = -1$ would indicate opposing ranks.

preference by collecting 5000 human image comparison annotations and applying the ranking model of [10]. We evaluate reward inference models in terms of how well they agree with this human labelling using Kendall's τ , a measure of the ordinal association between observation sets, and Spearman's ρ , a measure of rank correlation. Fig. 7 shows these results.

We benchmark probabilistic temporal ranking (PTR) against a maximum entropy reward model with both a Gaussian process prior (GP-ME-VAE*) [23] and a neural network prior (Deep-ME-VAE*) [40], a monotonically increasing linear temporal ranking model (LTR) [3] and a servoing reward model (Servo-VAE*) based on the cosine similarity of a latent image embedding to a final image captured. We also include a number of ablation results for probabilistic temporal ranking models. Model parameters are provided in the appendices.

Here, VAE* denotes the use of pre-trained image embedding learned independently using variational autoencoding, ML-PTR refers to a model trained without decoding the latent embedding (no autoencoder loss), ML-PTR-VAE refers to a maximum likelihood model trained jointly with both a variational autoencoding and pairwise ranking objective, and GP-PTR-VAE* denotes the use of the probabilistic temporal ranking with a pre-trained image embedding. It should be noted that all reward models were inferred without policy search, by directly optimising the reward objective.

It is clear that PTR outperforms baseline approaches. The maximum entropy reward models fail to learn adequate reward models. Servoing proved somewhat effective, but is unlikely to scale to more general problems and use cases. PTR improves upon LTR, illustrating the importance of allowing for non-monotonically increasing rewards.

The ablation results show that variational-autoencoding produces better reward models. This is most likely due to its regularising effect, which helps to avoid over-fitting to insignificant image appearance differences. Directly optimising without this regularising effect (ML-PTR) essentially results

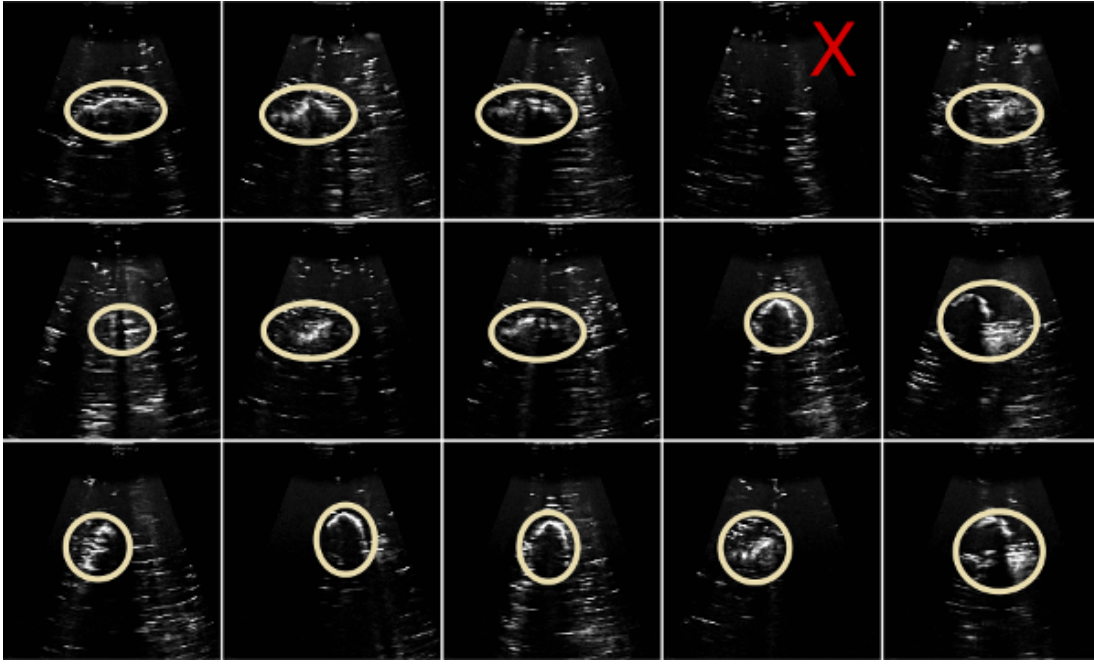
in a monotonically increasing reward model, and produces similar results to LTR. Interestingly, learning an independent auto-encoding and using a single layer bottleneck reward network or Gaussian process, proved to be an extremely effective strategy.

We believe that maximum entropy reward inference fails for two primary reasons. First, probabilistic temporal ranking produces substantially more training data, as each pair of images sampled (50 000 pairs) from a demonstration provides a supervisory signal. In contrast, the maximum entropy approach treats an entire trajectory as a single data point (10 trajectories), and thus needs to learn from far fewer samples, which is made even more challenging by the high dimensional image inputs. Secondly, the maximum entropy reward assumes that frequently occurring features are a sign of a good policy, which means that it can mistakenly associate undesirable frames seen during the scan's searching process for frames of high reward.

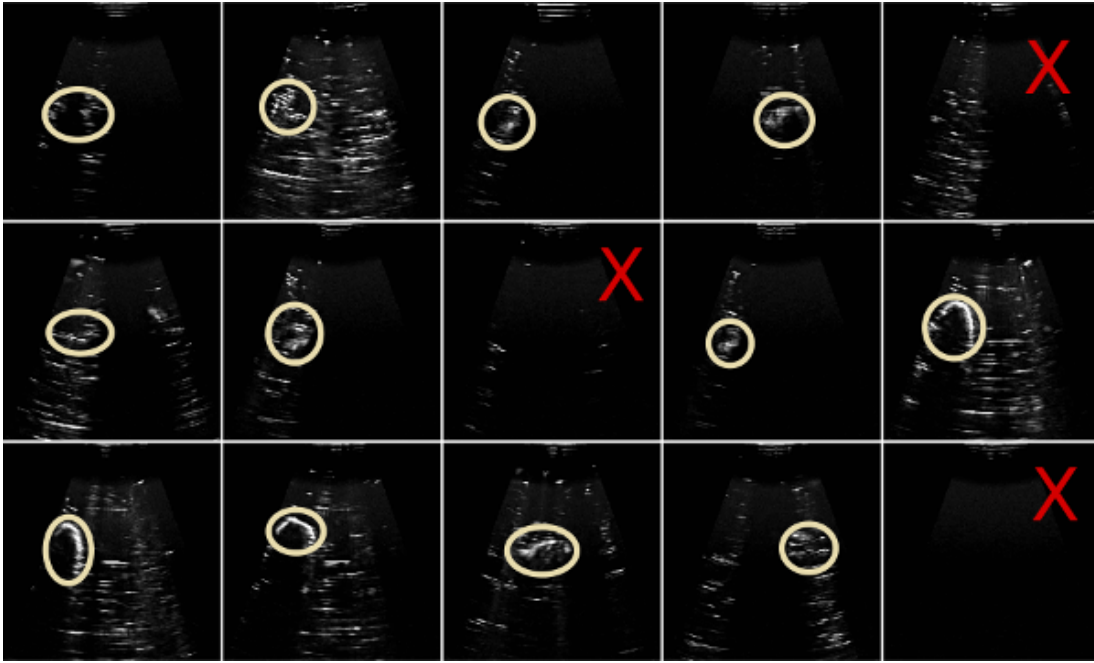
V. POLICY EVALUATION

For policy evaluation, we compare probabilistic temporal ranking with a Gaussian process maximum entropy inverse reinforcement learning approach. For both models we use the same latent feature vector (extracted using a stand-alone variational autoencoder following the architecture in Fig. 6), and the same Bayesian optimisation policy to ensure a fair comparison. We compare the two approaches by evaluating the final image captured during scanning, and investigating the reward traces associated with each model.

Trials were repeated 15 times for each approach, alternating between each, and ultrasound gel was replaced after 10 trials. Each trial ran for approximately 5 minutes, and was stopped when the robot pose had converged to a stable point, or after 350 frames had been observed. A high quality ultrasound scan is one in which the contours of the target object stand out as high intensity, where the object is centrally located in a scan,



(a) Probabilistic temporal ranking reward (Average human image rating: 0.254 ± 0.079)



(b) Maximum entropy reward (Average human image rating: 0.119 ± 0.198)

Fig. 8. Final images obtained after policy convergence clearly show that images obtained using probabilistic temporal ranking are much clearer and capture the target object far more frequently than the maximum entropy reward. Target objects are circled, failures marked with a cross. (Images are best viewed electronically, with zooming. See anonymous companion site, <https://sites.google.com/view/ultrasound-scanner>, for higher resolution images.)

and imaged clearly enough to give some idea of the target object size (see Fig. 2).

As shown in Fig. 8, the probabilistic temporal ranking model consistently finds the target object in the phantom, and also finds better rated images. Mean and standard deviations in image ratings were obtained using the rating model (see above) trained for reward evaluation using human image preference comparisons. The maximum entropy approach fails more frequently than the ranking approach, and when detection

is successful, tends to find off-centre viewpoints, and only images small portions of the target object.

It is particularly interesting to compare the reward traces for the probabilistic temporal ranking model to those obtained using maximum entropy IRL when the Bayesian optimisation scanning policy is applied. Fig. 9 overlays the reward traces obtained for each trial. The maximum entropy reward is extremely noisy throughout trials, indicating that it has failed to adequately associate image features with reward. Similar

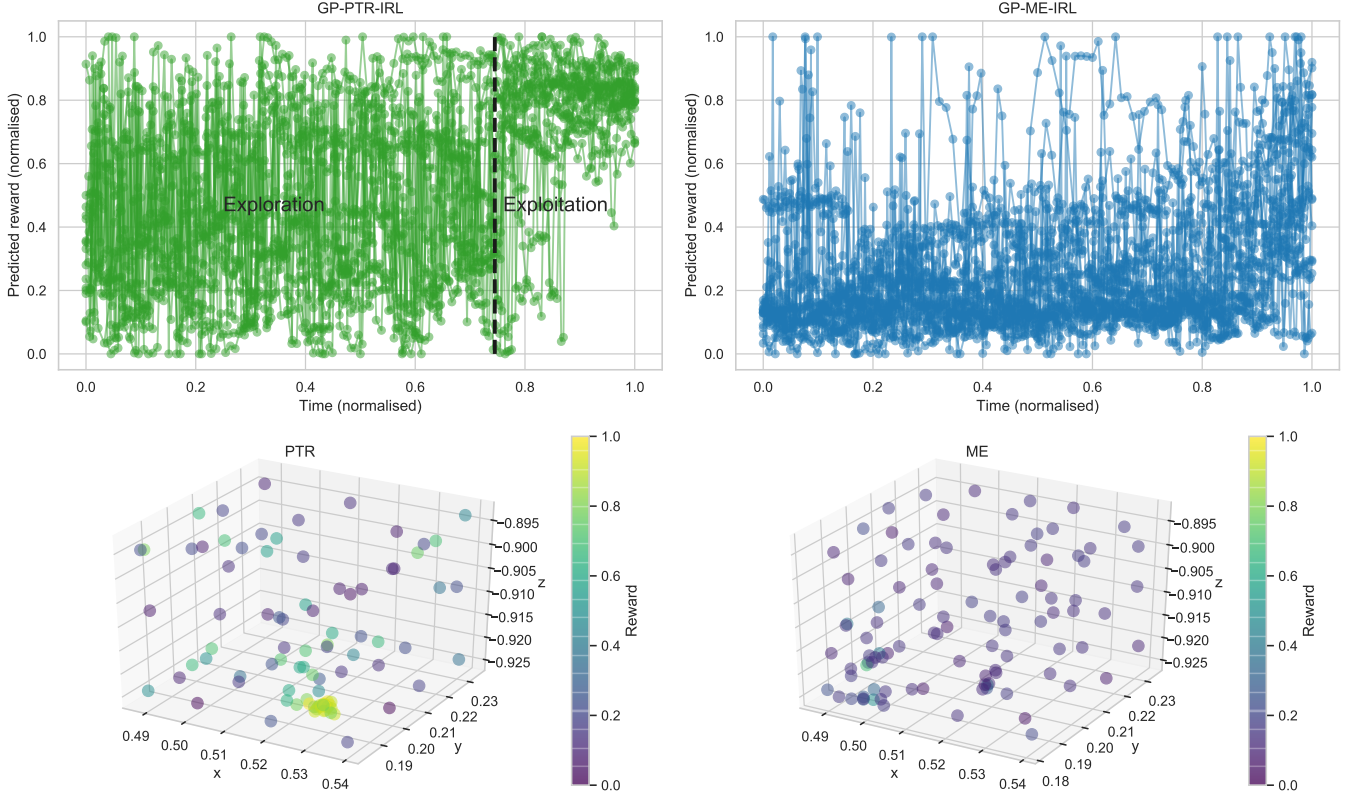


Fig. 9. Reward traces (top) show that the probabilistic temporal ranking reward is stable enough for the BO robot policy to explore the volume of interest (varying reward) before exploiting (stable reward). The maximum entropy reward is extremely noisy, indicating that it has failed to consistently associate high quality ultrasound image features with reward. This can also be observed when the 3D positions selected by the Bayesian optimisation policy are visualised (bottom), and coloured by the reward associated with the ultrasound images obtained when visiting these locations. The PTR policy first explores the allowable search region, before converging to an optimal viewing position (the cluster of high reward points). A policy using the maximum entropy reward model fails to locate the target object.

images fail to consistently return similar rewards, so the Bayesian optimisation policy struggles to converge to an imaging position with a stable reward score. In contrast, the reward trace associated with the pairwise ranking model contains an exploration phase where the reward varies substantially as the robot explores potential viewpoints, followed by a clear exploitation phase where an optimal viewpoint is selected and a stable reward is returned.

Fig. 10 shows the predicted reward over the search volume (a 50 mm x 50 mm x 30 mm region above the imaging phantom) for a PTR trial, determined as part of the Bayesian optimisation search for images with high reward, from reward and position samples (see Fig. 9). Here, we capture images at 3D end-effector locations according to the Bayesian optimisation policy, and predict the reward over the space of possible end-effector states using (7). Importantly, the Gaussian process proxy function is able to identify an ultrasound positioning region associated with high reward. This corresponds to a position above the target object, where the contact force with the phantom is firm enough to press through air pockets, but light enough to maintain a thin, air-tight layer of gel between the probe and phantom.

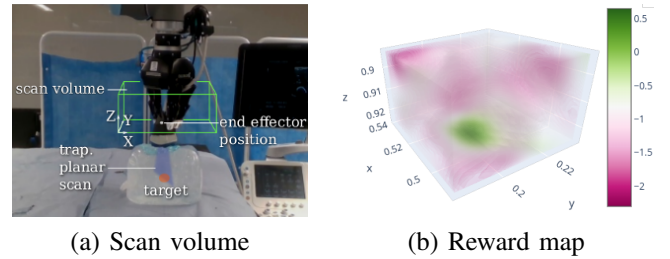


Fig. 10. A visualisation of the reward map (b) inferred by our method (Section IV-A) during scanning shows that it attributes high rewards (green) when the probe is pressed against the container directly above the target. The scan volume, or the support of the reward map, is illustrated using a green wireframe in the setup (a).

VI. CONCLUSION

This work introduces an approach to inverse optimal control or reinforcement learning that infers rewards using a probabilistic temporal ranking approach. Here, we take advantage of the fact that demonstrations, whether optimal or sub-optimal, generally involve steps taken to improve upon an existing state. Results show that leveraging this to infer reward through a ranking model is more effective than common IRL methods in sub-optimal cases where demonstrations require a period of discovery in addition to reward exploitation and when observation traces are high dimensional.

This paper also shows how the proposed reward inference

model can be used for a challenging ultrasound imaging application. Here, we learn to identify image features associated with target objects using kinesthetic scanning demonstrations that are sub-optimal, as they inevitably require a search for an object and position or contact force that returns a good image. Using this within a policy that automatically searches for positions⁴ and contact forces that maximise a learned reward, allows us to automate ultrasound scanning.

When comparing with human scanning, a primary challenge we have yet to overcome is that of spreading ultrasound gel smoothly over a surface. Human demonstrators implicitly spread ultrasound gel evenly over a target as part of the scanning process so as to obtain a high quality image. The Gaussian process policy used in this work is unable to accomplish this, which means scans are still noisier than those taken by human demonstrators. Moreover, human operators typically make use of scanning parameters like image contrast, beam width and scanning depth, which we kept fixed for these experiments. Nevertheless, the results presented here show extensive promise for the development of targeted automatic ultrasound imaging systems, and open up new avenues towards semi-supervised medical diagnosis.

ACKNOWLEDGMENTS

This work is supported by funding from the Turing Institute, as part of the Safe AI for surgical assistance project. We are particularly grateful to the Edinburgh RAD group and Dr Paul Brennan for valuable discussions and recommendations.

APPENDIX A

MAXIMUM LIKELIHOOD ARCHITECTURE PARAMETERS

Convolutional VAE	
Batch size	128
Training epochs	100
Adam optimiser	learning rate = $1e-4$
Input dims	$112 \times 112 \times 1 \in (0, 1)$
Encoder	
Conv 32	5×5 kernel, relu, strides 2
Conv 64	5×5 kernel, relu, strides 2
Conv 128	5×5 kernel, relu, strides 2
Conv 256	5×5 kernel, relu, strides 2
Dense FC	1024 neurons, relu
Dense FC	16×2 output (mean, variance)
Decoder	
Dense FC	1024 neurons, relu
Conv transpose 128	5×5 kernel, relu, strides 2
Conv transpose 64	5×5 kernel, relu, strides 2
Conv transpose 32	6×6 kernel, relu, strides 2
Conv transpose 1	6×6 kernel, relu, strides 2
Output dims	$112 \times 112 \times 1 \in (0, 1)$
Reward predictor	
Dense FC	relu, output dims 1

REFERENCES

[1] Pieter Abbeel and Andrew Y Ng. Apprenticeship learning via inverse reinforcement learning. In *Proceedings of the twenty-first international conference on Machine learning*, page 1. ACM, 2004.

⁴See <https://sites.google.com/view/ultrasound-scanner> for videos and higher resolution scan images, along with links to code.

[2] P. Abolmaesumi, S. E. Salcudean, Wen-Hong Zhu, M. R. Sirospour, and S. P. DiMaio. Image-guided control of a robot for medical ultrasound. *IEEE Transactions on Robotics and Automation*, 18(1):11–23, Feb 2002.

[3] Daniel Angelov, Yordan Hristov, Michael Burke, and Subramanian Ramamoorthy. Composing Diverse Policies for Temporally Extended Tasks. *Robotics and Automation Letters (RA-L)*, 2020.

[4] J. Andrew (Drew) Bagnell. An Invitation to Imitation. Technical Report CMU-RI-TR-15-08, Carnegie Mellon University, Pittsburgh, PA, March 2015.

[5] Jonathan Binney and Gaurav S Sukhatme. Branch and bound for informative path planning. In *2012 IEEE International Conference on Robotics and Automation*, pages 2147–2154, 2012.

[6] Abdeslam Boularias, Jens Kober, and Jan Peters. Relative entropy inverse reinforcement learning. In *Proceedings of the Fourteenth International Conference on Artificial Intelligence and Statistics*, pages 182–189, 2011.

[7] Darius Braziunas and Craig Boutilier. Preference elicitation and generalized additive utility. *AAAI*, 21(2), 2006.

[8] Eric Brochu, Tyson Brochu, and Nando de Freitas. A Bayesian interactive optimization approach to procedural animation design. In *Proceedings of the 2010 ACM SIGGRAPH/Eurographics Symposium on Computer Animation*, pages 103–112. Eurographics Association, 2010.

[9] Daniel Brown, Wonjoon Goo, Prabhat Nagarajan, and Scott Niekum. Extrapolating Beyond Suboptimal Demonstrations via Inverse Reinforcement Learning from Observations. In *International Conference on Machine Learning*, pages 783–792, 2019.

[10] Michael Burke, Siyabonga Mbonambi, Purity Molala, and Raesetje Sefala. Rapid Probabilistic Interest Learning from Domain-Specific Pairwise Image Comparisons. *arXiv preprint arXiv:1706.05850*, 2017.

[11] R. Calandra, A. Seyfarth, J. Peters, and M. P. Deisenroth. An experimental comparison of Bayesian optimization for bipedal locomotion. In *2014 IEEE International Conference on Robotics and Automation (ICRA)*, pages 1951–1958, May 2014.

[12] P. Chatelain, A. Krupa, and M. Marchal. Real-time needle detection and tracking using a visually servoed 3D ultrasound probe. In *2013 IEEE International Conference on Robotics and Automation*, pages 1676–1681, May 2013.

[13] Doo-Hyun Cho, Jung-Su Ha, Sujin Lee, Sunghyun Moon, and Han-Lim Choi. Informative path planning and mapping with multiple UAVs in wind fields. In *Distributed Autonomous Robotic Systems*, pages 269–283. Springer, 2018.

[14] Wei Chu and Zoubin Ghahramani. Preference learning with gaussian processes. In *Proceedings of the 22nd international conference on Machine learning*, pages 137–144, 2005.

[15] Marc Deisenroth and Carl E Rasmussen. PILCO: A model-based and data-efficient approach to policy search. In *Proceedings of the 28th International Conference on machine learning (ICML-11)*, pages 465–472, 2011.

- [16] Chelsea Finn, Paul Christiano, Pieter Abbeel, and Sergey Levine. A connection between generative adversarial networks, inverse reinforcement learning, and energy-based models. *arXiv preprint arXiv:1611.03852*, 2016.
- [17] Justin Fu, Katie Luo, and Sergey Levine. Learning robust rewards with adversarial inverse reinforcement learning. *International Conference on Learning Representations (ICLR)*, 2018.
- [18] Seyed Kamyar Seyed Ghasemipour, Richard Zemel, and Shixiang Gu. A Divergence Minimization Perspective on Imitation Learning Methods. *Conference on Robot Learning (CoRL)*, 2019.
- [19] Ralf Herbrich, Tom Minka, and Thore Graepel. TrueSkill: a Bayesian skill rating system. In *Advances in neural information processing systems*, pages 569–576, 2007.
- [20] Jonathan Ho and Stefano Ermon. Generative adversarial imitation learning. In *Advances in neural information processing systems*, pages 4565–4573, 2016.
- [21] M Hadi Kiapour, Kota Yamaguchi, Alexander C Berg, and Tamara L Berg. Hipster wars: Discovering elements of fashion styles. In *European conference on computer vision*, pages 472–488. Springer, 2014.
- [22] Alp Kucukelbir, Dustin Tran, Rajesh Ranganath, Andrew Gelman, and David M Blei. Automatic differentiation variational inference. *The Journal of Machine Learning Research*, 18(1):430–474, 2017.
- [23] Sergey Levine, Zoran Popovic, and Vladlen Koltun. Nonlinear inverse reinforcement learning with Gaussian processes. In *Advances in Neural Information Processing Systems*, pages 19–27, 2011.
- [24] T. Li, O. Kermorgant, and A. Krupa. Maintaining visibility constraints during tele-echography with ultrasound visual servoing. In *2012 IEEE International Conference on Robotics and Automation*, pages 4856–4861, May 2012.
- [25] Kaicheng Liang, Albert J. Rogers, Edward D. Light, Daniel von Allmen, and Stephen W. Smith. Three-Dimensional Ultrasound Guidance of Autonomous Robotic Breast Biopsy: Feasibility Study. *Ultrasound in Medicine & Biology*, 36(1):173 – 177, 2010.
- [26] Chun Kai Ling, Kian Hsiang Low, and Patrick Jaillet. Gaussian process planning with Lipschitz continuous reward functions: Towards unifying Bayesian optimization, active learning, and beyond. In *Thirtieth AAAI Conference on Artificial Intelligence*, 2016.
- [27] Manuel Lopes, Francisco Melo, and Luis Montesano. Active learning for reward estimation in inverse reinforcement learning. In Wray Buntine, Marko Grobelnik, Dunja Mladenić, and John Shawe-Taylor, editors, *Machine Learning and Knowledge Discovery in Databases*, pages 31–46, Berlin, Heidelberg, 2009. Springer Berlin Heidelberg.
- [28] Anirudha Majumdar, Sumeet Singh, Ajay Mandlekar, and Marco Pavone. Risk-sensitive Inverse Reinforcement Learning via Coherent Risk Models. In *Proceedings of Robotics: Science and Systems*, Cambridge, Massachusetts, July 2017.
- [29] R. Marchant and F. Ramos. Bayesian Optimisation for informative continuous path planning. In *2014 IEEE International Conference on Robotics and Automation (ICRA)*, pages 6136–6143, May 2014.
- [30] R. Martinez-Cantin. Bayesian optimization with adaptive kernels for robot control. In *2017 IEEE International Conference on Robotics and Automation (ICRA)*, pages 3350–3356, May 2017.
- [31] Ruben Martinez-Cantin, Nando de Freitas, Eric Brochu, José Castellanos, and Arnaud Doucet. A Bayesian exploration-exploitation approach for optimal online sensing and planning with a visually guided mobile robot. *Autonomous Robots*, 27(2):93–103, 2009.
- [32] Nikhil Naik, Jade Philipoom, Ramesh Raskar, and César Hidalgo. Streetscore – predicting the perceived safety of one million streetscapes. In *Proceedings of the IEEE Conference on Computer Vision and Pattern Recognition Workshops*, pages 779–785, 2014.
- [33] Radford M Neal. Priors for infinite networks. In *Bayesian Learning for Neural Networks*, pages 29–53. Springer, 1996.
- [34] Andrew Y Ng, Stuart J Russell, et al. Algorithms for inverse reinforcement learning. In *Icml*, volume 1, page 2, 2000.
- [35] John Salvatier, Thomas V. Wiecki, and Christopher Fonnesbeck. Probabilistic programming in Python using PyMC3. *PeerJ Computer Science*, 2:e55, April 2016.
- [36] Pierre Sermanet, Corey Lynch, Yevgen Chebotar, Jasmine Hsu, Eric Jang, Stefan Schaal, Sergey Levine, and Google Brain. Time-contrastive networks: Self-supervised learning from video. In *2018 IEEE International Conference on Robotics and Automation (ICRA)*, pages 1134–1141, 2018.
- [37] Hiroaki Sugiyama, Toyomi Meguro, and Yasuhiro Minami. Preference-learning based inverse reinforcement learning for dialog control. In *Thirteenth Annual Conference of the International Speech Communication Association*, 2012.
- [38] Christopher KI Williams and Carl Edward Rasmussen. *Gaussian processes for machine learning*, volume 2. MIT press Cambridge, MA, 2006.
- [39] Christian Wirth, Riad Akrou, Gerhard Neumann, and Johannes Fürnkranz. A survey of preference-based reinforcement learning methods. *The Journal of Machine Learning Research*, 18(1):4945–4990, 2017.
- [40] Markus Wulfmeier, Peter Ondruska, and Ingmar Posner. Maximum entropy deep inverse reinforcement learning. *arXiv preprint arXiv:1507.04888*, 2015.
- [41] Zhengkun Yi, Roberto Calandra, Filipe Veiga, Herke van Hoof, Tucker Hermans, Yilei Zhang, and Jan Peters. Active tactile object exploration with Gaussian processes. In *2016 IEEE/RSJ International Conference on Intelligent Robots and Systems (IROS)*, pages 4925–4930, 2016.
- [42] Brian D Ziebart, Andrew Maas, J Andrew Bagnell, and Anind K Dey. Maximum entropy inverse reinforcement learning. In *Proceedings of AAAI’08 Proceedings of the 23rd national conference on Artificial intelligence*, volume 3, pages 1433–1438, 2008.